Massive Thymic Deletion Results in Systemic Autoimmunity through Elimination of CD4$^+$ CD25$^+$ T Regulatory Cells

Fei F. Shih, Laura Mandik-Nayak, Brian T. Wipke, and Paul M. Allen

Department of Pathology and Immunology Washington University School of Medicine, St. Louis, MO 63110

Abstract

Incomplete deletion of KRN T cells that recognize the ubiquitously expressed self-antigen glucose-6-phosphate-isomerase (GPI) initiates an anti-GPI autoimmune cascade in K/BxN mice resulting in a humorally mediated arthritis. Transgenic (Tg) expression of a KRN T cell receptor (TCR) agonist under the major histocompatibility complex class II promoter resulted in thymic deletion with loss of anti-GPI T and B cell responses and attenuated arthritis course. However, double Tg mice succumbed to systemic autoimmunity with multiorgan inflammation and autoantibody production. Extensive thymic deletion resulted in lymphopenia and elimination of CD4$^+$ CD25$^+$ regulatory T cells (Tregs), but spared some CD4$^+$ T cells expressing endogenous TCR, which oligoclonally expanded in the periphery. Disease was transferred by these T cells and prevented by cotransfer of CD4$^+$ CD25$^+$ Tregs. Moreover, we extended our findings to another TCR system (anti–hen egg lysozyme [HEL] TCR/HEL mice) where similarly extensive thymic deletion also resulted in disease. Thus, our studies demonstrated that central tolerance can paradoxically result in systemic autoimmunity through differential susceptibility of Tregs and autoreactive T cells to thymic deletion. Therefore, too little or too much negative selection to a self-antigen can result in systemic autoimmunity and disease.

Key words: autoimmunity • thymic deletion • arthritis • T regulatory cells • TCR transgenic

Introduction

K/BxN is a murine model of spontaneous rheumatoid arthritis that mimics many of the clinical and histologic features of human disease with synovitis predominantly in the distal small joints and systemic features of hypergammaglobulinemia and splenomegaly (1). K/BxN mice were generated by crossing KRN TCR transgenic (Tg) mice with nonobese diabetic (NOD) mice. Although the initial specificity of the KRN TCR was directed to RNase(42–56)/I-A^k, KRN TCR also recognizes peptides 281–293 of the glycolytic enzyme, glucose-6-phosphate-isomerase (GPI) bound to I-A^{g7} (2). Failure of complete T cell tolerance allows KRN T cells to become activated by endogenously presented GPI and to provide help to anti-GPI B cells, giving rise to arthritogenic autoantibodies. These autoantibodies are necessary and sufficient for the induction of synovitis, as transfer of anti-GPI antibodies into most strains of mice resulted in disease (3). Extensive serum transfer studies have provided important insights into the pathogenesis of the joint disease through the deposition of arthritogenic anti-GPI antibodies and subsequent recruitment of inflammatory mediators into the joints (4, 5). However, it is still unclear how anti-GPI T and B cells persist in the mature lymphocyte pool despite the ubiquitous nature of this autoantigen. As KRN T cells serve as the catalyst to ignite this autoimmune cascade, we have focused our attention on the negative selection of KRN T cells.

To investigate the role of antigen presentation in the failure in T cell selection, we have generated a Tg mouse expressing a peptide mimic of GPI(281–293) termed G7m under the control of the MHC II promoter. Accordingly, we showed G7mTg splenocytes to be potent stimulators of KRN T cells, signifying effective presentation of the transgene-encoded agonist. As expected, KRN/G7mTg double Tg mice exhibited a greatly attenuated arthritis course with concomitant loss of anti-GPI T and B cell responses. Surprisingly, KRN/G7mTg mice succumbed to a

The online version of this article contains supplemental material.

Address correspondence to Paul M. Allen, Department of Pathology and Immunology, Washington University School of Medicine, Campus Box 8118, 660 South Euclid Avenue, St. Louis, MO 63110. Phone: (314) 362-8758; Fax: (314) 362-8888; email: allen@wustl.edu

B.T. Wipke's present address is Elan Pharmaceuticals, Inc., 800 Gateway Boulevard, Building 800, Room 154B, South San Francisco, CA 94080.

Abbreviations used in this paper: ANA, antinuclear antibodies; d3Ntx, day 3 neonatally thymectomized; GI, gastrointestinal; GPI, glucose-6-phosphate-isomerase; HEL, hen egg lysozyme; mHEL, membrane form of HEL; NOD, nonobese diabetic; SP, single positive; Tg, transgenic; Treg, regulatory T cell.

 J. Exp. Med. © The Rockefeller University Press • 0022-1007/2004/02/323/13 $8.00
Volume 199, Number 3, February 2, 2004 323–335
http://www.jem.org/cgi/doi/10.1084/jem.20031137

systemic autoimmunity with multiorgan inflammation and autoantibody production. Expression of the TCR ligand resulted in severe deletion of T cells bearing transgene-encoded TCR, leaving behind autoreactive $CD4^+$ T cells using endogenous TCRs. $CD4^+$ $CD25^+$ regulatory T cells (Tregs) were reduced in the double Tg mice, suggesting loss of Tregs as a mechanism of disease. Significantly, cotransfer of $CD4^+$ $CD25^+$ Tregs prevented induction of disease achieved via transfer of splenocytes from double Tg mice. Taken together, our studies demonstrated that central tolerance can paradoxically result in systemic autoimmunity through differential susceptibility of Tregs and autoreactive T cells to thymic deletion.

Materials and Methods

Mice. The Tg mouse line (G7mTg) expresses a membrane form of hen egg lysozyme (HEL; mHEL) containing the KRN agonist peptide G7m(GKKVATFVHAGYG) as an epitope tag. G7m was previously shown to stimulate KRN T cells with 10–100-fold increased sensitivity compared with the GPI(281–293) (2). This is due to increased binding to $I\text{-}A^{g7}$ relative to the native GPI(281–293) peptide (6). The mHEL/G7m transgene construct was generated by PCR mutagenesis of the previously described mHEL/Hb(64–76) transgene construct using nonoverlapping oligonucleotides: 5′-CACGCTGGATACGGAAACCGTAACAC-CGATGGGAGTACCGAC-3′ (coding) and 5′-CACGAAGG-TCGCCACCTTTTTGCCTGTAGCCTGGGTGTTG-3′ (noncoding). Nucleotides encoding the G7m peptide are underlined. Sequencing in both directions confirmed the replacement of Hb(64–76) with G7m peptide. Transgene expression is driven by the Eα promoter that has been previously demonstrated to effectively target transgene expression in MHC II^+ cells (7). A 5.2-kb BglI fragment containing the Eα promoter and the mHEL/G7m chimeric gene was isolated and injected into the male pronuclei of fertilized B6.AKR oocytes. Seven founders were identified by flow cytometry using the mHEL-specific antibody F10.6.6 (8). G7mTg7 and G7mTg5 mice were used in this study. Transgene expression was 63–75% of MHC II^+ splenocytes in G7mTg7 and ~10% in G7mTg5 splenocytes (unpublished data). These were bred to KRN TCR Tg mice with specificity for GPI(281–293)/$I\text{-}A^{g7}$ or to 3A9 TCR Tg mice which are specific for HEL(46–61)/$I\text{-}A^k$. The resulting progeny were screened by PCR analysis of tail DNA. All progeny were heterozygous for the relevant transgenes.

KRN TCR Tg mice on a C57BL/6 background have been described (1). KRN Tg mice were bred to congenic B6.AKR ($H\text{-}2^k$ background) to generate KRN^k mice, which are homozygous for $H\text{-}2^k$. KRN^k mice were crossed to $G7mTg^k$ mice to generate KRN/$G7mTg^k$ mice, which are then bred to NOD mice to generate $KRN^{k/g7}$ and KRN/$G7mTg^{k/g7}$ mice on an $H\text{-}2^{k/g7}$ heterozygous background. B6.G7 denotes congenic C57BL/6 mice expressing $I\text{-}A^{g7}$. These were crossed to KRN/$G7mTg^k$ to generate congenic KRN/B6.G7 and KRN/G7mTg/B6.G7 mice expressing $H\text{-}2^{k/g7}$ with pure B6 genetic background. NOD mice were purchased from Taconic. All mice were bred and housed under specific pathogen-free conditions in the animal facility at the Washington University Medical Center.

Primary T Cell Proliferation. Proliferation assays were performed in triplicate with unfractionated T cells (5×10^5 cells/well) from the spleen and LNs in Iscove's medium containing 10% heat-inactivated fetal calf serum, 2 mM Glutamax (GIBCO BRL), 2×10^{-5} M β-mercaptoethanol, and 50 μg/ml gentamicin (ISC-10) in round-bottom 96-well plates (Costar). Splenic APCs received 2,000 rad γ irradiation before use. Cultures were pulsed at 72 h with 0.2 μCi [^{3}H]thymidine/well and harvested 18–24 h later. Proliferation was measured as counts per minute incorporated.

In Vitro Suppression Assay. T cell proliferation was assayed as described above with sorted $CD4^+$ $CD25^+$ and $CD4^+$ $CD25^-$ T cells (at 5×10^4 cells/well) from $KRN^{k/g7}$ mice being cultured separately or mixed at 1:1 in 96-well round-bottom plates with 5×10^5 irradiated T cell–depleted $H\text{-}2^{k/g7}$ splenic APCs.

Arthritis and Wasting Incidence. Mice were assessed weekly for synovitis of the rear and front paws for 4 mo. Ankle thickness was measure axially across the malleoli using a Fowler Metric Pocket Thickness Gauge (Ralmikes Tool-A-Rama). Ankle thickness was rounded off to the nearest 0.05 mm. Mice were weighed weekly using a miniscale. Wasting is defined clinically as fur ruffling, hunched posture, and weight loss >20%. Mice were killed when moribund or weight fell below 12 g (<50% mean weight of control).

Anti-GPI ELISA. Mice were bled weekly and sera were stored at −20°C before analysis. Sera were diluted at 1:100 in PBS, 1% BSA, and 0.1% Tween 20 and plated in Immunlon II plates (Fisher Biotech) coated with 2 μg/ml GPI-GST as previously described (9). Donkey anti–mouse horseradish peroxidase (Jackson ImmunoResearch Laboratories) was used as a secondary antibody. The assay was detected using 2,2′-Azino-di-(3-ethylbenathiazoline sulfonate) diammonium salt (ABTS substrate; Roche Molecular Biochemicals). Absorbance was measured at 414 nm.

Antinuclear Antibodies (ANA). Sera was diluted at 1:100 in PBS. 50 μl diluted serum sample was applied to immobilized Hep2 cells (Antibodies Inc.) and *Crithidia luciliae* (Antibodies Inc.). Anti–mouse IgG-FITC and anti–mouse IgM-FITC were used as secondary antibodies. ANA and *Crithidia* staining were read independently by two readers. Positive controls were sera from MRL/lpr mice.

Anti-RBC Antibody. Sera was diluted at 1:50 in FACS® buffer (PBS, 1% BSA, and 0.1% NaN_3). 50 μl diluted sera was used to stain B6.AKR RBCs and was detected with anti–mouse IgG-FITC and anti–mouse IgM-FITC for flow cytometric analysis. Positives were defined as staining >3× background.

RF ELISA. This RF ELISA made use of allotypic difference between the capture Ig (a allotype) and sample IgG of b allotype. Sera were diluted at 1:100 in PBS, 1% BSA, and 0.1% Tween 20 and plated in Immunlon II plates (Fisher Biotech) coated with 2 μg/ml $IgG2a^a$ (HOPC-1). A cocktail of biotinylated antibodies comprising of anti-IgM (11/41), anti-$IgG2a^b$ (5.7), and anti-$IgG1^b$ (B68-2; 2 μg/ml each), followed by SAV–horseradish peroxidase, was used for detection. HOPC-1, 11/41, 5.7, and B68-2 were purchased from Southern Biotechnology Associates, Inc. As b allotype–specific antibodies were available for only the IgG2a and IgG1 isotypes, RFs of the IgG2b or IgG3 isotypes were not detected. Hence, the RF measurement was likely to be an underestimate. The assay was developed using ABTS substrate. Positive was defined as OD > 3× background.

Flow Cytometry. Single cell suspensions of thymocytes, splenocytes, and LN cells ($1–2 \times 10^6$) were surface stained according to standard protocols. The following antibodies/reagents were used: GK1.5-PE, GK1.5-FITC (anti-CD4), 53-6.7–FITC (anti-CD8), RR4-7–biotin (anti-Vβ6), 14.4.4-FITC (anti-$I\text{-}E^k$), PC61-PE (anti-CD25), MEL-14–PE (anti–CD62-L), PgP-1–FITC (anti-CD44), H1.2F3-FITC (anti-CD69), streptavidin-

PerCP (BD Biosciences), F10.6.6-biotin (HEL specific), 1G12-biotin (3A9 clonotype specific), and streptavidin-PE (Caltag). TCR Vβ usage was determined by flow cytometry using a panel of 15 FITC-conjugated TCR Vβ-specific antibodies from BD Biosciences. All samples were analyzed on a FACScalibur™ flow cytometer (BD Biosciences) with CELLQuest™ software. Gating on live lymphocytes was based on forward and side scatter and/or exclusion of propidium iodide. 50–500,000 gated events were collected per sample.

Quantitative PCR. $CD4^+$ T cells were enriched from the spleen and LN cells from three to five 4-wk-old $KRN^{k/k}$ or $KRN^{k/g7}$ mice using anti-CD4 microbeads (Miltenyi Biotec) according to the manufacturer's directions. $CD4^+$ single positive (SP) thymocytes were isolated by complement-mediated depletion of $CD8^+$ thymocytes using anti-CD8 antibody 3.166. $CD4^+$ $CD25^+$ and $CD4^+$ $CD25^-$ T cells were sorted using the FACS Vantage™ after labeling with anti–GK1.5-FITC and PC61-PE. Typically, 0.5×10^6 $CD4^+$ $CD25^+$ T cells and 0.2×10^6 $CD4^+$ $CD25^+$ thymocytes were isolated from three to five mice. mRNA was isolated using TRIzol (Invitrogen) extraction and was treated with DNase I for 15 min at 25°C. First strand cDNA was generated using oligo-dT primers via TaqMan Reverse Transcription kit (Applied Biosystems) according to the manufacturer's directions. Real-time PCR for FoxP3 was measured as previously described (10) using TaqMan Universal Master Mix (Applied Biosystems). CD25 and HPRT PCR were performed as previously described (11) using SYBR Master Mix (Applied Biosystems). PCR was performed in 25 μl with cycling conditions as previously described (10). Data were collected using ABI Prism 7700 Sequence Detection System Software. A standard curve was generated with a dilution series (1:1, 1:10, 1:100, 1:1,000, 1:10,000, and 1:100,000) of a reference cDNA sample that was run at the same time as the unknown samples. CD25 and FoxP3 expression were normalized to HPRT mRNA.

Transfer Studies. Spleens were harvested from 5–12-wk-old 3A9 or 3A9/G7mTg mice. Single cell suspension was generated by RBC lysis. Unfractionated splenocytes ($30–40 \times 10^6$) from one spleen were injected intravenously into each 4–6-wk-old B6.AKR or congenic $RAG1^{-/-}$ mouse. Equivalent numbers of T cells from 3A9 or 3A9/G7mTg mice were transferred. $CD4^+$ $CD25^+$ T cells comprised 1.5% ($4.5–6 \times 10^5$) and <0.2% ($<7 \times 10^4$) of total transferred cells from 3A9 and 3A9/G7mTg mice. Mice were followed weekly for weight loss and clinical evidence of disease.

For the cotransfer experiments, 5×10^5 $CD4^+$ $CD25^+$ or $CD4^+$ $CD25^-$ T cells were purified from 3A9 mice via MACS (Miltenyi Biotec) separation according to the manufacturer's directions and injected intravenously into each $RAG1^{-/-}$ mouse 24 h before transfer of 3A9/G7m splenocytes. Some mice received 20×10^6 $CD4^+$ $CD25^-$ T cells purified from 3A9 mice.

Online Supplemental Material. Fig. S1 demonstrates the expression of the mHEL/G7m transgene on I-E^k–expressing cells in the thymic medulla of mHEL/G7mTg7 mice. Fig. S2 depicts the time course of wasting of representative KRN/G7mTg (Fig. S2 A) and 3A9/mHELTg (Fig. S2 B) mice. Fig. S3 illustrates the splenomegaly and disrupted splenic architecture seen in KRN/G7mTg7 mice. Figs. S1–S3 are available at http://www.jem.org/cgi/content/full/jem.20031137/DC1.

Results

Generation of mHEL/G7mTg Mice. To address the role of antigen insufficiency in thymic tolerance, we sought to augment thymic presentation of the peptide ligands recognized by KRN T cells. We first attempted to generate Tg mice that express GPI(281–293) as an epitope tag in a fusion protein consisting of HEL and the L^d transmembrane domain (designated mHEL). Transgene expression is driven by the Eα promoter to target expression on APCs in the thymus and periphery (7). This strategy had been successfully used by our laboratory previously to express Hb(64–76) and its analogs in the thymus for selection of Hb-specific T cells (8). Although mHEL/Hb chimeric proteins incorporating Hb(64–76) and its analogs were stably expressed on cell surfaces, similar mHEL/GPI chimeras were unstable, making expression studies problematic. To circumvent this difficulty, we used a GPI(281–293) mimic, G7m, which was structurally based on Hb(64–76), strongly stimulated KRN T cells (2), and proved to be stably expressed as mHEL/G7m chimeric proteins. Using this approach, seven Tg lineages on a B6.AKR ($H\text{-}2^k$) background were obtained, and one line, designated G7mTg7, was used in the majority of the studies described herein.

The transgene was expressed in the majority of MHC II^+ cells in the spleen, LN, and thymus. In the thymus, mHEL/G7m chimeric molecules were expressed most highly in the medulla, coinciding with MHC II^+ cells (Fig. S1, top, available at http://www.jem.org/cgi/content/full/jem.20031137/DC1). Hence, we showed that the transgene was appropriately targeted to thymic medullary cells, which have previously been shown to be exquisitely effective at mediating thymic negative selection (12).

Moreover, when we bred G7mTg7 mice to NOD mice to introduce the I-A^{g7} molecule, the resultant $G7mTg7^{k/g7}$ splenocytes provoked vigorous proliferation of KRN^k T cells in comparison to the modest response elicited by transgene-negative and NOD splenocytes (Fig. 1). Indeed, expression

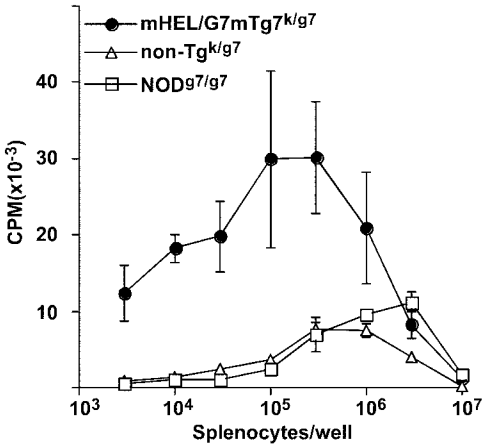

Figure 1. mHEL/G7m splenocytes are potent stimulators of KRN T cells. Graded numbers of unfractionated irradiated splenocytes from $mHEL/G7mTg7^{k/g7}$ (●), $nontransgenic^{k/g7}$ (△), and $NOD^{g7/g7}$ (□) mice were cultured with 5×10^5 KRN^k T cells in 96-well round-bottom plates for 72 h with 0.2 μCi [^{3}H]thymidine in the last 18 h. Each point represents the mean of triplicate wells with error bars indicating SD. Data are representative of four independent experiments.

of the mHEL/G7m transgene augmented T cell stimulation by 1,000-fold relative to that achieved with endogenous GPI, highlighting the enhanced presentation of the KRN TCR ligand through our targeted transgene approach.

G7m Transgene Expression Abrogates Arthritis in KRN/G7mTg7$^{k/g7}$ Mice. KRN$^{k/g7}$ and KRN/G7mTg7$^{k/g7}$ mice were followed for the onset and severity of arthritis starting at 4 wk of age. Arthritis initiated in KRN$^{k/g7}$ mice between 4–5 wk of age underwent a robust acute inflammatory phase, peaked at 6–8 wk, and settled to a chronic phase where ankle deformity predominated and the inflammation was relatively quiescent (Fig. 2 A). In contrast, arthritis in the KRN/G7mTg7$^{k/g7}$ mice followed a greatly attenuated course both in terms of severity and penetrance. Although 100% of KRN$^{k/g7}$ mice exhibited symmetrical involvement of all four limbs, KRN/G7mTg7$^{k/g7}$ mice showed heterogeneous presentation with asymmetrical swelling of one or two isolated limbs in ~40% of mice. The remainder had swelling on the dorsum of the paws or no synovitis at all. Among those with synovitis, the acute inflammatory phase was foreshortened to 1–2 wk and did not leave any residual limb deformity. Neither control G7mTg7$^{k/g7}$ nor transgene-negative littermates showed any arthritis (unpublished data).

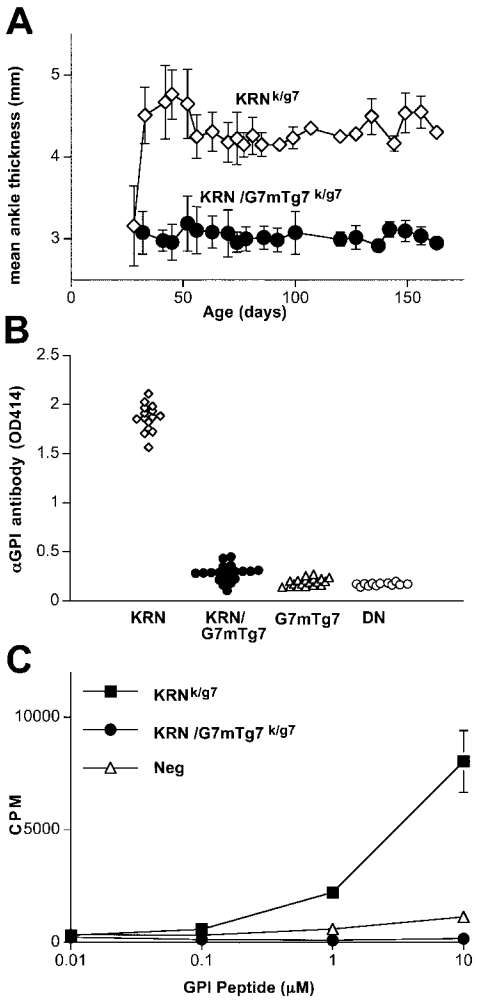

Figure 2. KRN/G7mTg7$^{k/g7}$ mice exhibited reduced arthritis and anti-GPI antibodies. (A) Mean ankle thickness ± SD of 6 KRN$^{k/g7}$ (◇) and 10 KRN/G7mTg7$^{k/g7}$ (●) mice. Data are representative of 20 KRN$^{k/g7}$ and 16 KRN/G7mTg7$^{k/g7}$ mice derived from 14 separate litters of mice collected over a 6-mo period. (B) Absorbance of anti-GPI ELISA of KRN$^{k/g7}$ (◇), KRN/G7mTg7$^{k/g7}$ (●), G7mTg7$^{k/g7}$ (△), and double negative (DN; ○) mice (n = 15, 20, 23, and 12, respectively). Sera from 8-wk-old mice were diluted at 1:100 and serum anti-GPI was detected by ELISA. Each symbol represents an individual mouse. (C) T cell proliferation in response to GPI(281–293). 5 × 10^5 splenocytes from KRN$^{k/g7}$ (■), KRN/G7mTg7$^{k/g7}$ (●), and transgene-negative (△) mice were cultured with graded doses of GPI(281–293) peptide with 2 × 10^5 irradiated H-2$^{k/g7}$ splenocytes in 96-well round-bottom plates for 72 h with 0.2 μCi [^{3}H]thymidine in the last 18 h. Each point represents the mean of triplicate wells with error bars indicating SD. Data are representative of three independent experiments.

As anti-GPI antibodies are the causative agents in initiating joint inflammation, we showed an attendant decrease in the production of anti-GPI antibodies in KRN/G7mTg7$^{k/g7}$ mice (Fig. 2 B). This low anti-GPI titer was maintained through later time points and serum was insufficient to elicit disease when transferred into BALB/c mice (unpublished data).

Next, we assessed T cell response to GPI(281–293) in KRN/G7mTg7$^{k/g7}$ mice relative to their KRN$^{k/g7}$ littermate. In contrast to the residual but significant GPI reactivity exhibited by KRN$^{k/g7}$ splenocytes, no proliferation was elicited from splenocytes isolated from KRN/G7mTg7$^{k/g7}$ mice (Fig. 2 C). Hence, GPI-specific T cells were functionally eliminated. Taken together, overexpression of the KRN TCR agonist abrogated arthritis and anti-GPI B and T cell responses, demonstrating effective T cell tolerance of KRN T cells in KRN/ G7mTg7$^{k/g7}$ mice.

KRN/G7mTg7$^{k/g7}$ Mice Develop Multiorgan Inflammation. Surprisingly, KRN/G7mTg7$^{k/g7}$ mice developed multiorgan systemic autoimmunity. Starting at 10–12 wk of age, the mice exhibited wasting, manifested as ruffled fur, scaly skin, hunched posture, colitis, and weight loss. By 100 d of age, 50% of the KRN/G7mTg7$^{k/g7}$ (n = 16) mice had succumbed to wasting. A representative time course is presented in Fig. S2 A, available at http://www.jem.org/cgi/content/full/jem.20031137/DC1. The remaining mice became progressively affected, such that by 6 mo of age only 20% remained. With the exception of arthritis in KRN$^{k/g7}$ mice, KRN$^{k/g7}$ (n = 20) and G7mTg7$^{k/g7}$ (n = 15) mice were otherwise healthy throughout this time course.

A survey of multiple organs from 4–20-wk-old KRN/G7mTg7$^{k/g7}$ mice revealed involvement of the liver, kidneys, lungs, heart, pancreatic islets, salivary glands, thyroid, and gastrointestinal (GI) tract. No histologic inflammation was seen in the muscle, skin, brain, ovaries, and testes. Two patterns of inflammatory infiltrates were observed. The first was well-organized perivascular infiltrates comprised of T and B cells, as well as neutrophils, seen in the liver, kidneys, lungs, pancreatic islets, and salivary glands (Fig. 3, A–C, and unpublished data). In the more affected organs, the infiltrates eroded through the vessel walls with resultant vasculitis occluding the lumen. The organ parenchyma was relatively spared as there was no hepatocellular necrosis or

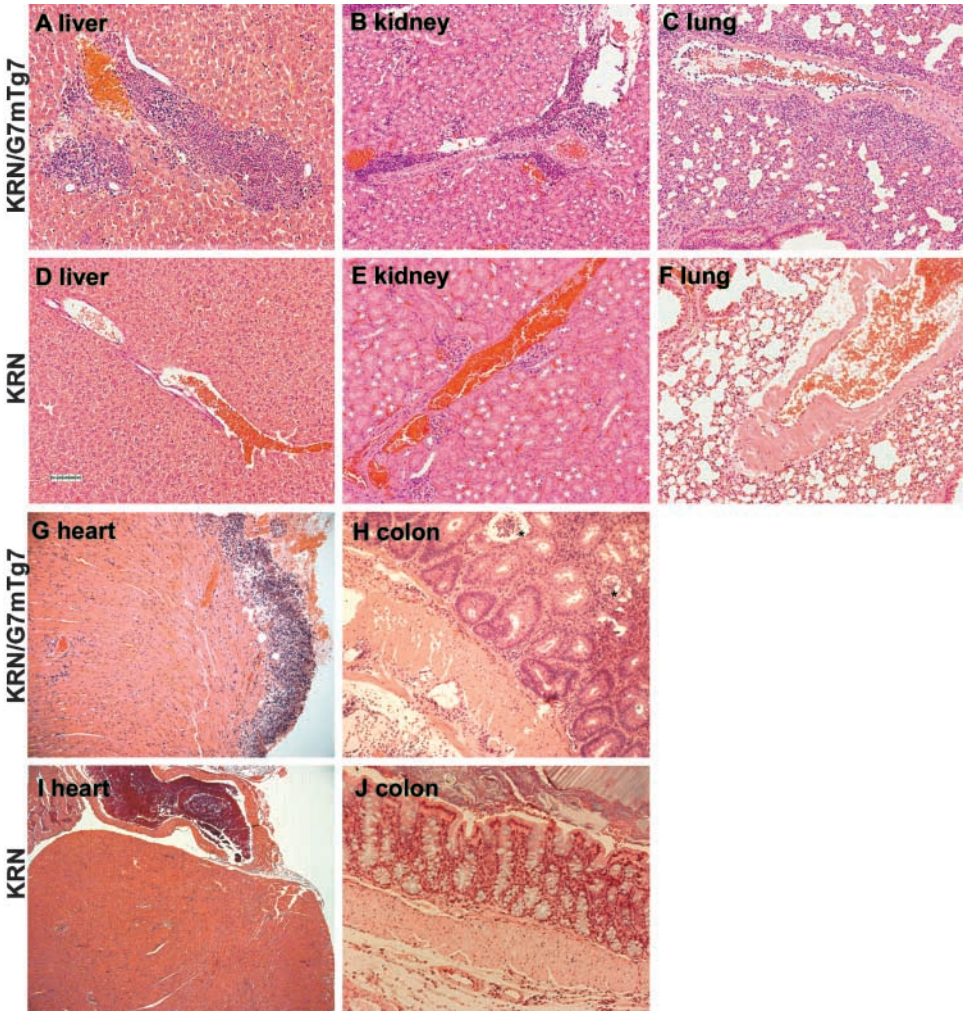

Figure 3. KRN/G7mTg7$^{k/g7}$ mice displayed inflammation in multiple organs. We examined 10 KRN/G7mTg7$^{k/g7}$ mice (7 aged 8–12 wk, 2 aged 16–20 wk, 1 aged 4 wk), 8 KRN mice (7 aged 8–12 wk, 1 aged 4 wk), and 2 G7mTg7$^{k/g7}$ mice (both 8–10 wk) for histological evidence of autoimmunity. Paraffin sections of liver (A and D), kidneys (B and E), lungs (C and F), heart (G and I), and colon (H and J) from 2-mo-old KRN/G7mTg7$^{k/g7}$ (A–C, G, and H) and KRN$^{k/g7}$ (D–F, I, and J) mice are stained with hematoxylin and eosin. *, crypt abscesses. ×100. Bar, 100 μM.

glomerulonephritis. These perivascular lesions were observed in all the KRN/G7mTg7$^{k/g7}$ mice as early as 4 wk of age, albeit to a lesser degree.

The second inflammatory pattern was a more invasive infiltrate seen in the heart and the GI tract (Fig. 3, G and H). The heart exhibited an intense neutrophilic pericarditis with lymphocytic myocarditis (Fig. 3 G). However, the most severely affected organ was the GI tract, particularly the distal bowel (cecum and colon). Inflammatory bowel disease was in all probability the major cause of mortality in the KRN/G7mTg7$^{k/g7}$ mice as colitis preceded wasting in the affected mice. The severe diffuse colitis typical of the colon and cecum is shown in Fig. 3 H. Multiple ulcerations eroded through the wall of the mesentery with focal peritonitis. The normal colonic architecture was replaced by a robust influx of neutrophils, mast cells, and plasma cells into the lamina propria with formation of crypt abscesses. Significantly, the gastric mucosa and parietal cells appeared unaffected.

KRN$^{k/g7}$ mice exhibited inflammatory infiltrates in the periarticular regions as previously reported (1). Of the multiple visceral organs surveyed in 8 KRN$^{k/g7}$ mice, perivascular infiltrates in the lungs were seen in one 3-mo-old mouse. No other pathologic abnormality was evident (Fig. 3, D–F, I, and J). Organs from control G7mTg7$^{k/g7}$ mice were notably normal.

To exclude infection as the cause of the inflammation, KRN/ G7mTg7$^{k/g7}$ mice were screened and were negative for respiratory and enteric pathogens including rodent *Helicobacter spp.* with the exception of lactose-negative *Escherichia coli*. Thus, by overexpressing the KRN TCR ligand in MHC II^{+} cells, the disease phenotype was diverted from a largely joint-centered disease to a lethal multiorgan systemic inflammation.

Splenomegaly with Extramedullary Hematopoiesis in KRN/G7mTg7$^{k/g7}$ Mice. KRN/G7mTg7$^{k/g7}$ mice displayed significant splenomegaly, two- to fourfold greater than their KRN$^{k/g7}$ littermates (Fig. S3 A, available at http://www.jem.org/cgi/content/full/jem.20031137/DC1). The anatomic distinction between red and white pulp in the spleen was obliterated by the presence of exuberant extramedullary hematopoiesis. No normal lymphoid follicles were discernible (Fig. S3, B and C, available at http://www.jem.org/cgi/content/full/jem.20031137/DC1). Correspondingly, complete blood counts and peripheral blood smears from KRN/G7mTg7$^{k/g7}$ mice revealed au-

Table I. *Clinical Features of KRN/G7mTg Mice, 3A9/G7mTg, and 3A9/JB5 Mice*

Mouse	TCR	Antigen	Number	αGPI	ANA	Wasting
KRN TCR						
KRN	KRN	—	20	20/20	0/20	0/20
KRN/G7mTg7	KRN	mHEL/G7m	16	0/16	16/16	8/16
KRN/G7mTg5	KRN	mHEL/G7m	10	0/10	10/10	5/10
G7mTg7	—	mHEL/G7m	13	0/13	0/13	0/13
G7mTg5	—	mHEL/G7m	15	0/15	0/15	0/15
DN	—	—	26	0/26	0/26	0/26
3A9 TCR						
3A9	3A9	—	25	NA	0/25	0/25
3A9/G7mTg7	3A9	mHEL/G7m	17	NA	7/17	16/17
3A9/G7mTg5	3A9	mHEL/G7m	16	NA	10/16	13/16
3A9/JB5	3A9	mHEL/Hb	14	NA	3/14	10/14
G7mTg7	—	mHEL/G7m	7	NA	0/7	0/7
G7mTg5	—	mHEL/G7m	7	NA	0/7	0/7
JB5	—	mHEL/Hb	19	NA	0/19	0/19
DN	—	—	36	NA	0/36	0/36

Litters of mice were followed for 4 mo with weekly weights and serial bleeds starting at 4 wk of age. Data are derived from 14 litters of KRN/G7mTg7$^{k/g7}$, 9 litters of KRN/G7mTg5$^{k/g7}$, 9 litters of 3A9/G7mTg7, 7 litters of 3A9/G7mTg5, and 13 litters of 3A9/JB5 mice. Detection for anti-GPI antibodies and ANA was performed as described in Materials and Methods. Wasting was defined as loss of >20% initial body weight. Colitis (manifesting as diarrhea and anal prolapse) accompanied wasting in a majority of the affected animals. DN, double negative; NA, not applicable.

toimmune hemolytic anemia and compensatory reticulocytosis. There was also markedly enhanced granulocytosis with elevated numbers of neutrophils and immature band forms in the peripheral blood, indicative of acute inflammation (unpublished data).

Autoantibody Production in KRN/G7mTg7 Mice. Given the disease involvement in multiple organ systems, we next assessed for the presence of autoantibodies commonly associated with systemic autoimmunity. Although KRN/G7mTg7$^{k/g7}$ mice did not produce anti-GPI antibodies, they were hypergammaglobulinemic (unpublished data) and produced autoantibodies of multiple specificities. ANA were detected in the sera of all the KRN/G7mTg7$^{k/g7}$ mice tested ($n = 30$), as early as 5 wk of age (before the onset of overt disease). The specificity of ANA was confirmed to be double stranded DNA by positive staining for the kinetoplast of *C. luciliae*. RF (anti-IgG antibodies) was detected in 67% of the KRN/G7mTg7$^{k/g7}$ mice ($n = 15$) in contrast to their absence in KRN$^{k/g7}$ mice. In addition, anti-RBC antibodies were detected in 50% of the KRN/G7mTg7$^{k/g7}$ sera ($n = 14$). The production of disease-associated autoantibodies was not the result of indiscriminate polyclonal B cell activation as antibodies to GPI or neoself-antigen, HEL, were not produced (unpublished data).

NOD Background Is Not Required for Disease Development. To ascertain whether the NOD background was necessary for disease manifestation, KRN/G7mTg7^{k} mice were bred to congenic B6.G7 mice to introduce I-A^{g7} while maintaining a pure B6 genetic background. Similar to KRN/G7mTg7$^{k/g7}$ mice, KRN/G7mTg7/B6G7$^{k/g7}$ mice did not develop arthritis but succumbed to multiorgan inflammation, colitis, hematologic abnormalities, and autoantibodies (ANA and RF). The tempo of disease was accelerated. All KRN/G7mTg7/B6.G7$^{k/g7}$ mice succumbed to wasting by 3 mo of age. Despite sharing some of the inflammatory changes of aged NOD mice, the systemic autoimmunity seen in KRN/G7mTg7$^{k/g7}$ mice did not require the NOD genetic background. Indeed, the NOD background genes conferred a degree of protection, as the disease course was less severe in the KRN/G7mTg7$^{k/g7}$ mice (B6xNOD background) compared with the KRN/G7mTg7/B6.G7$^{k/g7}$ mice (homozygous B6 background).

To exclude a transgene founder effect, KRN mice were crossed to another G7mTg line, designated G7mTg5. KRN/G7mTg5$^{k/g7}$ mice displayed a similar disease phenotype as KRN/G7mTg7$^{k/g7}$ mice with an attenuated arthritis course (Table I). They did not produce anti-GPI antibodies but produced ANA in all the mice assayed. KRN/G7mTg5$^{k/g7}$ mice also succumbed to the multiorgan disease seen in KRN/G7mTg7$^{k/g7}$ mice (Table I and Fig. S2 A, which is available at http://www.jem.org/cgi/content/full/jem.20031137/DC1).

Extensive Thymic Deletion in KRN/G7mTg7$^{k/g7}$ Mice. We had purposefully targeted expression of a KRN TCR agonist to APCs, including those in the thymus to alter the KRN T cell repertoire, resulting in unexpected autoimmunity. Thus, to ascertain the effect of G7m on T cell selection, T cells from thymi, LNs, and spleens of 4-wk-old KRN^{k},

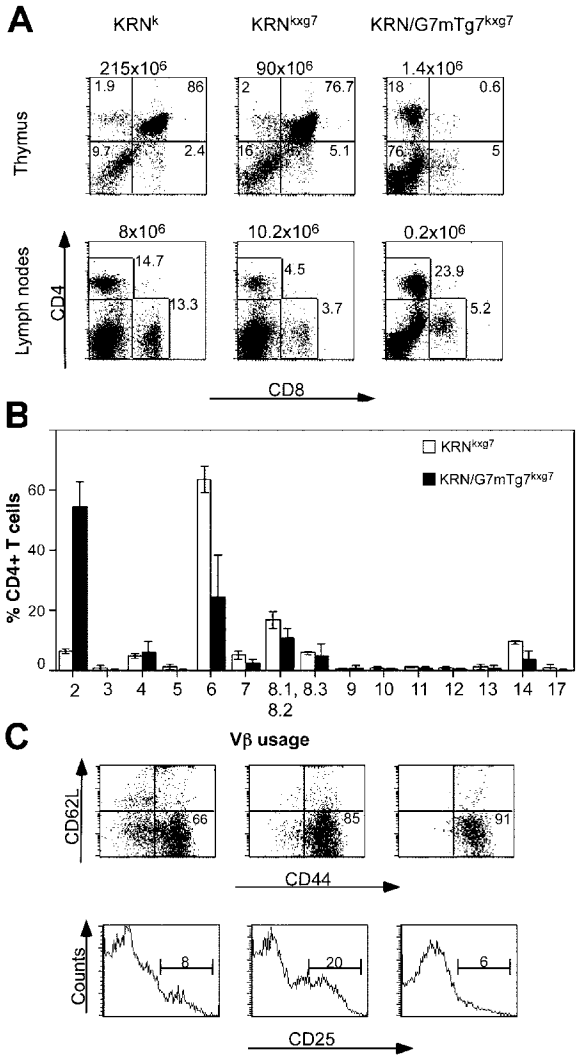

Figure 4. Deletion of Vβ6^{hi} CD4$^+$ T cells in KRN/G7mTg7$^{k/g7}$ mice. (A) CD4/CD8 profile of thymocytes and LN cells from KRN^k, KRN$^{k/g7}$, and KRN/G7mTg7$^{k/g7}$ mice. Cell numbers are displayed above each plot. Numbers in each panel indicate percent of cells. Average thymocyte numbers were 190 ± 56 × 10^6, 72 ± 34 × 10^6, and 1.9 ± 0.8 × 10^6, and average LN cell numbers were 16 ± 7.8 × 10^6, 23 ± 13 × 10^6, and 0.9 ± 0.8 × 10^6 in KRN^k, KRN$^{k/g7}$, and KRN/G7mTg7$^{k/g7}$ mice, respectively (n = 4). (B) Splenocytes from four KRN$^{k/g7}$ (□) and four KRN/G7mTg7$^{k/g7}$ (■) mice were analyzed by flow cytometry for TCR Vβ gene expression. Each data point represents mean percent of total CD4$^+$ T cells with error bar indicating ± SD. (C) CD4$^+$ splenocytes were gated and analyzed for activation markers CD44-FITC, CD62L-PE, and CD25-PE. Data are representative of three independent experiments.

KRN$^{k/g7}$, and KRN/G7mTg7$^{k/g7}$ mice were analyzed by flow cytometry. As T cells in KRN^k mice matured in the absence of I-A^{g7}, their T cell compartment and response were not subjected to negative selection by the endogenous GPI and therefore represented the baseline. Mice were analyzed before the onset of overt disease to minimize alterations to the T cell compartment due to systemic inflammation.

Consistent with negative selection, there was graded reduction of thymocyte numbers in KRN$^{k/g7}$ and KRN/G7mTg7$^{k/g7}$ mice relative to KRN^k mice (Fig. 4 A). Deletion of KRN T cells by endogenous GPI in KRN$^{k/g7}$ mice was relatively inefficient as the thymocyte numbers were reduced only threefold with preservation of the CD4/CD8 profile. In contrast, thymocyte deletion in KRN/G7mTg7$^{k/g7}$ mice was much more effective with a 100-fold reduction in total cellularity. Analysis of the CD4/CD8 compartments showed that the loss was primarily in the double positive thymocytes with preservation of CD4$^+$ SP thymocytes compared with the CD8$^+$ SP thymocytes.

The peripheral lymphoid compartments reflected the thymic constituents. At 4 wk of age, equivalent CD4$^+$ T cells were isolated from the LNs of KRN^k and KRN$^{k/g7}$ mice. In contrast, LNs in KRN/G7mTg7$^{k/g7}$ mice were atrophic and 10-fold fewer lymphocytes were recovered. These residual lymphocytes were predominantly CD4$^+$ T cells comprising 22.5–44.6% of total LN cells. As a clonotypic antibody to KRN was unavailable, we measured the expression of Vβ6 as a surrogate for the transgene-encoded TCR. We found that Vβ6 expression was decreased among the residual CD4$^+$ T cells in KRN$^{k/g7}$ and KRN/G7mTg7$^{k/g7}$ mice both in terms of frequency and level (unpublished data) as a consequence of negative selection. In KRN/G7mTg7$^{k/g7}$ mice, ~25% of the CD4$^+$ T cells expressed Vβ6 compared with 64% in KRN$^{k/g7}$ and 80% in KRN^k mice.

To determine the TCR usage in the remaining CD4$^+$ T cells, we conducted flow cytometric analysis using a panel of 15 Vβ-specific antibodies. There was a dramatic shift in the TCR repertoire such that >50% of the residual CD4$^+$ T cells in the KRN/G7mTg7$^{k/g7}$ mice used Vβ2 in contrast to 6.5% in the KRN$^{k/g7}$ mice (Fig. 4 B). There was no significant difference among the other endogenous Vβ genes. Vβ2$^+$ T cells were not selectively elevated in either G7mTg7 or non-Tg mice on the H-2$^{k/g7}$ background (unpublished data). It was plausible that the Vβ2 expansion resulted from aberrant thymic selection for HEL-specific T cells in KRN/G7mTg7$^{k/g7}$ mice. To address this possibility, we assayed for T cell proliferation in response to HEL protein and the five identified MHC II determinants of HEL. No HEL-specific T cell response was detected (unpublished data). Therefore, this oligoclonal expansion of Vβ2$^+$ T cells is likely a reflection of autoreactive T cells that had evaded deletion and expanded in response to self-antigen as had been seen in certain autoimmune disease such as experimental autoimmune encephalomyelitis (13).

CD4$^+$ T cells from KRN/G7mTg7$^{k/g7}$ and KRN$^{k/g7}$ mice displayed activation markers consistent with previous antigen exposure. In KRN$^{k/g7}$ mice, increased numbers of CD4$^+$ T cells were CD44^{hi} and CD62L^{lo} compared with KRN^k mice (Fig. 4 C). These data are consistent with the immune activation of KRN T cells by endogenous GPI. CD4$^+$ T cells in KRN/G7mTg7$^{k/g7}$ mice exhibited a further elevation in activation markers, such that 91% of the CD4$^+$ T cells were CD44^{hi} CD62L^{lo} (Fig. 4 C). In addition, these activated T cells exhibited elevated CD69 levels as well as increased cell volume by forward and side scatter (unpublished data).

Despite the activated phenotype of the CD4$^+$ T cells derived from KRN/G7mTg7$^{k/g7}$ mice, only 6% of these CD4$^+$ T cells were CD25^{hi}, whereas 20% of CD4$^+$ T cells

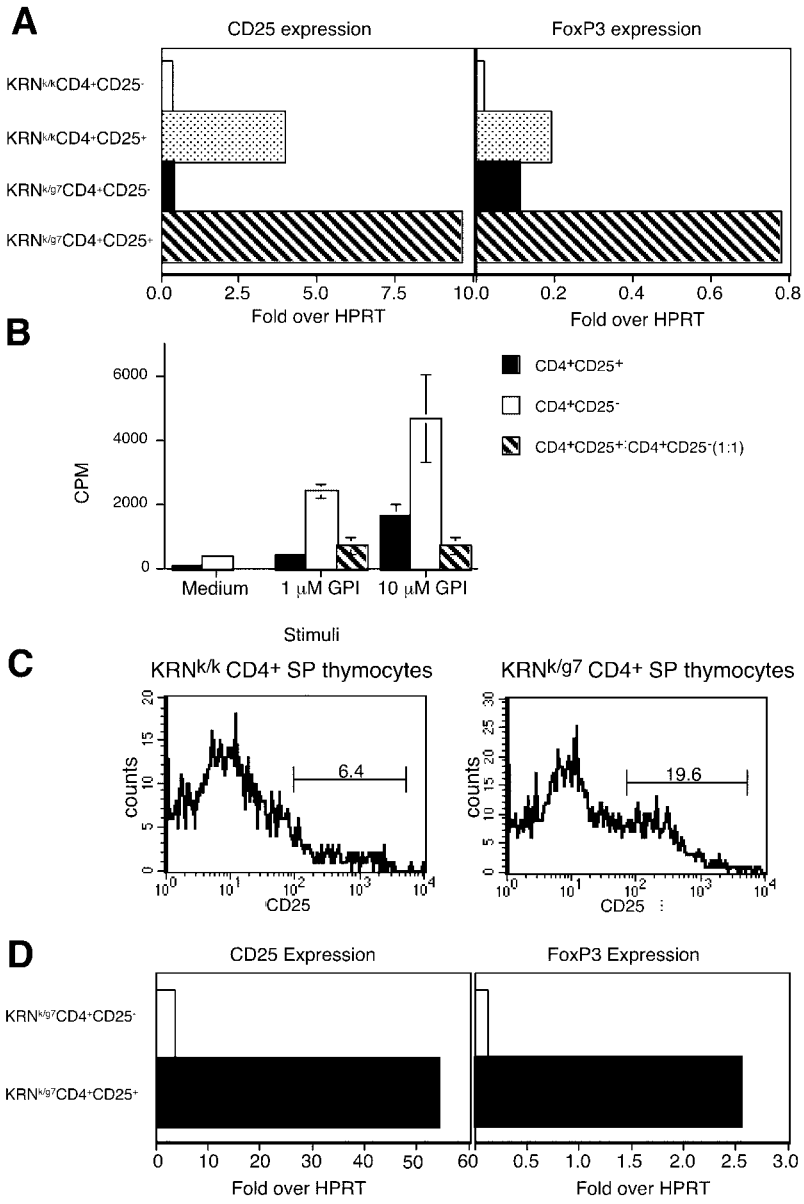

Figure 5. $CD4^+$ $CD25^+$ T cells from $KRN^{k/g7}$ mice are Tregs and are thymically derived. (A) Sorted $CD4^+$ $CD25^-$ (open and solid bars) and $CD4^+$ $CD25^+$ (dotted and striped bars) T cells from pooled LNs and spleens from three $KRN^{k/k}$ (open and dotted bars) and three $KRN^{k/g7}$ (solid and striped bars) mice were analyzed for HPRT, CD25, and FoxP3 expression by quantitative PCR and normalized to housekeeping gene HPRT. (B) Sorted $CD4^+$ $CD25^+$ and $CD4^+$ $CD25^-$ T cells were purified from pooled LNs and spleens of seven $KRN^{k/g7}$ mice. $CD4^+$ $CD25^+$ T cells (solid bars), $CD4^+$ $CD25^-$ (open bars), and mixed $CD4^+$ $CD25^+$/ $CD4^+$ $CD25^-$ (1:1; striped bars) were cultured at 5×10^4/well with graded doses of GPI(281–293) peptide and 2×10^5 irradiated T-depleted H-$2^{k/g7}$ splenocytes in 96-well round-bottom plates for 72 h with 0.2 μCi [^{3}H]thymidine in the last 18 h. Each point represents the mean of duplicate wells with error bars indicating SD. (C) Thymocytes from 4-wk-old $KRN^{k/k}$ and $KRN^{k/g7}$ mice were analyzed by flow cytometry with CD4-APC, CD8-FITC, and CD25-PE. Live cells were identified by propidium iodide exclusion. Histograms of CD25 expression of $CD4^+$ SP thymocytes are presented with the percentage of $CD25^{hi}$ cells indicated on the marker. Data are representative of three mice. (D) Sorted $CD4^+$ $CD25^-$ (open bars) and $CD4^+$ $CD25^+$ (solid bars) were purified from five $KRN^{k/g7}$ mice and analyzed for HPRT, CD25, and FoxP3 expression by quantitative PCR and normalized to HPRT.

from $KRN^{k/g7}$ mice were $CD25^{hi}$ (Fig. 4 C). As KRN T cells were activated by endogenous GPI in $KRN^{k/g7}$ mice, the enhanced $CD4^+$ $CD25^+$ T cells may reflect peripherally activated T cells or $CD4^+$ $CD25^+$ Tregs. To distinguish between these two possibilities, we assessed the expression of the forkhead transcription factor, FoxP3, by quantitative PCR. FoxP3 had been identified as critical in the development of $CD4^+$ $CD25^+$ Tregs (10, 11). $CD4^+$ $CD25^-$ and $CD4^+$ $CD25^+$ T cells were sorted from pooled LN cells and splenocytes from three to five $KRN^{k/k}$ and $KRN^{k/g7}$ mice. Expression of CD25 and FoxP3 were analyzed by quantitative PCR and normalized to the housekeeping gene HPRT. FoxP3 was expressed in low abundance but correlated with CD25 expression in both $KRN^{k/k}$ and $KRN^{k/g7}$ mice (Fig. 5 A). Moreover, to show that these are indeed Tregs, we assayed the ability of $CD4^+$ $CD25^+$ T cells from $KRN^{k/g7}$ mice to suppress the proliferation of their $CD4^+$ $CD25^-$ counterparts. $CD4^+$ $CD25^+$ T cells proliferated poorly in response to GPI compared to the response elicited in $CD4^+$ $CD25^-$ T cells. The addition of $CD4^+$ $CD25^+$ Tregs at a 1:1 ratio reduced proliferation by 70–85% (Fig. 5 B). Hence, $CD4^+$ $CD25^+$ T cells from $KRN^{k/g7}$ mice expressed FoxP3 and functioned as Tregs.

Consistent with the hypothesis that $CD4^+$ $CD25^+$ Tregs arose as a consequence of failed negative selection, we showed enhanced CD25 expression in $CD4^+$ SP thymocytes from $KRN^{k/g7}$ mice compared with $KRN^{k/k}$ mice ($19.9 \pm 0.8\%$ compared with $6.3 \pm 0.6\%$, respectively; Fig. 5 C). Moreover, FoxP3 expression was enriched among the $CD25^+$ population (Fig. 5 D). Taken together, our data demonstrated that $CD4^+$ $CD25^+$ T cells from $KRN^{k/g7}$ mice were thymically derived Tregs.

The paucity of $CD4^+$ $CD25^+$ T cells coupled with the severe thymic atrophy and lymphopenia in KRN/

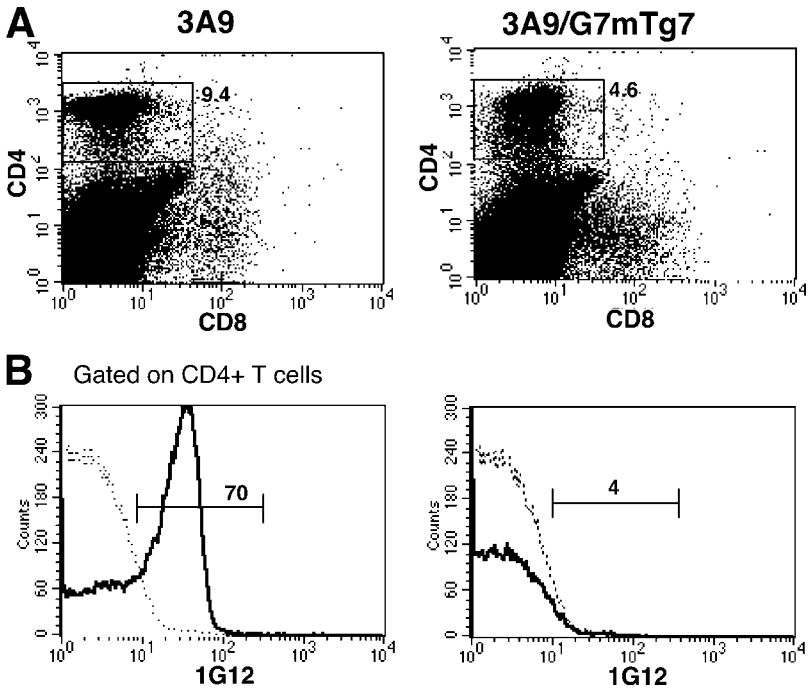

Figure 6. Clonotype$^+$ T cells are deleted in 3A9/G7mTg7 mice. Splenocytes from 3A9 and 3A9/G7mTg7 mice were analyzed by flow cytometry using CD4-PE, CD8-FITC, and 3A9-specific clonotypic antibody 1G12. Dot plot represents CD4 and CD8 expression. Clonotype expression of gated CD4$^+$ T cells are presented in the histograms as solid lines. Background staining of clonotype antibody of transgene-negative mouse is indicated by the dotted lines.

G7mTg7$^{k/g7}$ mice precluded similar analyses in these mice. In day 3 neonatally thymectomized (d3Ntx) mice, loss of CD4$^+$ CD25$^+$ Tregs was shown to result in systemic autoreactivity (14, 15). In light of the regulatory function exhibited by CD4$^+$ CD25$^+$ T cells from KRN$^{k/g7}$ mice and the similar disease manifestation seen in KRN/G7mTg7$^{k/g7}$ and d3NTx mice, our data suggest loss of Tregs as a mechanism for the systemic autoreactivity.

Systemic Autoimmunity Is Generalizable to Settings of Extensive Thymic Deletion. To determine if the disease phenotype was unique to KRN or was a generalizable phenomenon, we made use of 3A9 TCR Tg that recognizes HEL. Moreover, as HEL is a component of the mHEL/G7m transgene and clonotypic antibody to the 3A9 TCR is available, we could directly examine negative selection of 3A9 in mHEL/G7m. Accordingly, 3A9 TCR Tg mice were crossed to both G7mTg lineages. Consistent with efficient thymic deletion, clonotype$^+$ 3A9 T cells were eliminated in 3A9/G7mTg mice (Fig. 6). As summarized in Table I and Fig. S2 B, which is available at http://www.jem.org/cgi/content/full/jem.20031137/DC1, both lineages of 3A9/G7mTg mice succumbed to disease with wasting, colitis, dermatitis, and autoantibody production starting at 9–10 wk of age. Compared with KRN/G7mTg$^{k/g7}$ mice, 3A9/G7mTg mice displayed a higher frequency of wasting and colitis (80–94 vs. 50%) and lower frequency of autoantibody production. ANA were produced in 40–60% of 3A9/G7mTg mice and developed at a later time (8–12 wk). Histologically, 3A9/G7mTg mice also displayed multiorgan inflammation, albeit in only a subset of target organs (lungs, liver, and GI tract).

To eliminate the possibility of confounding effects of G7m or its transgene expression pattern, we made use of JB5 mice that expressed the mHEL/Hb chimeric protein on all MHC II$^+$ cells in the thymus and spleen (8) and at higher levels compared with G7mTg7$^{k/g7}$ mice (unpublished data). Despite higher mHEL transgene expression, the T cell compartments were identical to 3A9/G7m mice (unpublished data). In our previous report on 3A9/JB5 mice, we had not observed any pathology (8). In retrospect, that analysis was performed on 4–6-wk-old mice. However, by following the mice over a longer time course, we found that a majority of 3A9/JB5 Tg mice (70%) developed dermatitis and wasting by 12–16 wk of age (Fig. S2 B, available at http://www.jem.org/cgi/content/full/jem.20031137/DC1). ANA production was found only in 20% of the mice and these arose at late time points of >12 wk. Hence, the disease phenotype appeared to be a general phenomenon of massive thymic deletion.

Transfer of 3A9/G7m Splenocytes Recapitulates Disease Phenotype. Next, we ascertained whether the disease is transferable by splenocytes. We made use of the 3A9 system where the expression of the cognate antigen can be controlled. Accordingly, unfractionated splenocytes from 3A9/G7mTg mice were transferred into B6.AKR mice. Control mice received unfractionated 3A9 splenocytes. Mice were monitored weekly by clinical appearance and weight. Transfer of 3A9/G7mTg splenocytes into B6.AKR mice did not induce disease. Recipients remained healthy and continued to gain weight compared to control mice that received 3A9 splenocytes (Fig. 7 A). Failure to transfer disease may result from a requirement for mHEL/G7m expression in the host or active suppression by host lymphocytes. As the reduction of CD4$^+$ CD25$^+$ T cells in the KRN/G7mTg7$^{k/g7}$ mice suggested the loss of Tregs as a mechanism accounting for the systemic autoimmunity seen in these double Tg mice, we repeated the experiment using immunodeficient RAG1$^{-/-}$ hosts. Transfer of 3A9/

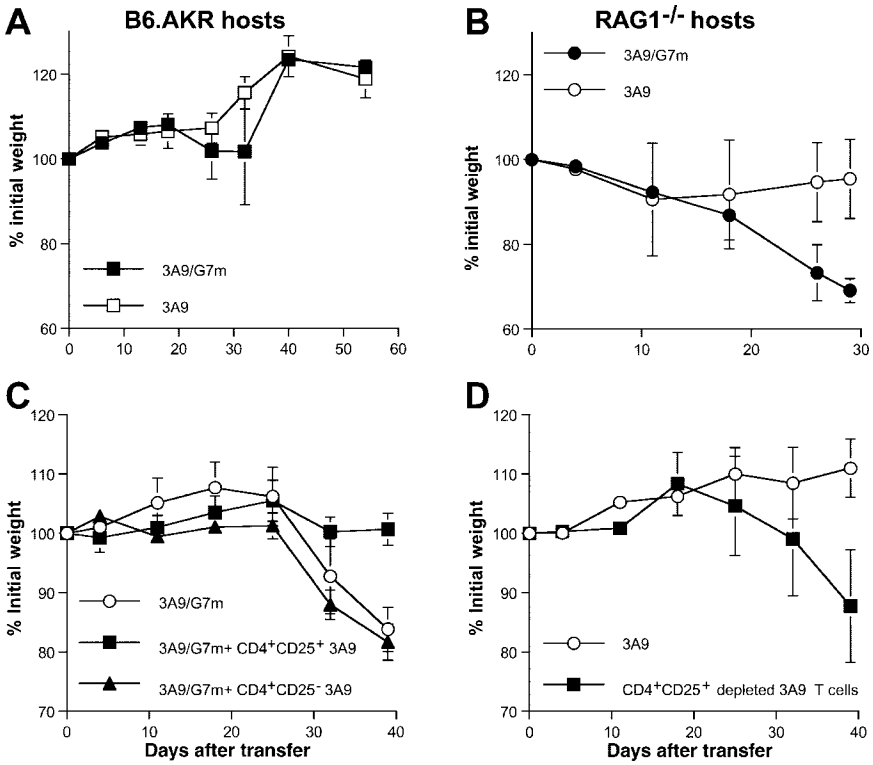

Figure 7. Wasting disease is transferable by 3A9/G7mTg splenocytes into immunodeficient hosts but not immunocompetent hosts. (A) Unfractionated 3A9 (□) and 3A9/G7m (■) splenocytes were transferred into B6.AKR mice (n = 3/group). Each data point represents the mean percent of initial weight with error bars indicating SD. (B) Unfractionated 3A9 (○) and 3A9/G7m (●) splenocytes were transferred into RAG1$^{-/-}$ mice (n = 3/group). Each data point represents the mean percent of initial weight with error bars indicating SD. (C) Unfractionated 3A9/G7m (○, ■, ▲) splenocytes were transferred into RAG1$^{-/-}$ mice. 5 × 10^5 CD4$^+$ CD25$^+$ (■) or CD4$^+$ CD25$^-$ (▲) splenocytes from 3A9 mice were transferred 24 h before the transfer of 3A9/G7m splenocytes. (D) Unfractionated 3A9 splenocytes (○) or 2 × 10^7 3A9 CD4$^+$ T cells depleted of CD4$^+$ CD25$^+$ T cells (■) were transferred into RAG1$^{-/-}$ mice. Each data point represents the mean percent of initial weight of three mice with error bars indicating SD. Data are representative of three independent experiments for A and B and two independent experiments for C and D.

G7mTg splenocytes into RAG1$^{-/-}$ mice recapitulated the disease phenotype present in 3A9/G7mTg mice. RAG1$^{-/-}$ mice that received 3A9/G7mTg splenocytes displayed steady weight loss with >25% weight loss by 24 d (Fig. 7 B). These mice were moribund and were killed. Histologic examination showed inflammatory changes in the liver, colon, and cecum similar to that seen in double Tg mice (unpublished data). RAG1$^{-/-}$ mice that received 3A9 splenocytes remained healthy. Moreover, the ability to transfer disease into host mice that do not express the mHEL/G7m transgene indicated that anti-HEL T cell response was not required for disease induction consistent with the loss of clonotype$^+$ T cells in 3A9/G7mTg mice. Therefore, the autoreactivity resulted from the specificity encoded by endogenously derived TCRs.

CD4$^+$CD25$^+$ Tregs Prevent Induction of Colitis. The differential ability to transfer disease into immunodeficient hosts but not immunosufficient hosts suggested active suppression of disease by host lymphocytes. Moreover, as 3A9 splenocytes also did not induce disease, we reasoned that they must contain inhibitory lymphocytes. Thus, to directly test the hypothesis that the absence of CD4$^+$ CD25$^+$ T cells from 3A9/G7mTg mice was responsible for the disease, we used two approaches. First, CD4$^+$ CD25$^+$ T cells from 3A9 mice were cotransferred into RAG1$^{-/-}$ mice with 3A9/G7mTg splenocytes and mice were monitored for weight loss. As shown in Fig. 7 C, cotransfer of CD4$^+$ CD25$^+$ T cells prevented the wasting evident in RAG1$^{-/-}$ mice that received 3A9/G7mTg splenocytes alone. Cotransfer of CD4$^+$ CD25$^-$ T cells failed to prevent disease. By a complementary approach, transfer of CD4$^+$ T cells from 3A9 mice that were depleted of CD4$^+$ CD25$^+$ T cells induced wasting (Fig. 7 D). Taken together, our data demonstrated the absence of a regulatory population in the 3A9/G7mTg mice as a critical factor in the pathogenesis of the systemic autoimmunity. In addition, as CD4$^+$ T cells from 3A9 mice were clonotype$^+$, Tregs derived from 3A9 mice were therefore HEL specific. As pathogenic 3A9/G7mTg T cells could mediate disease in mice lacking HEL, their target antigens represent as yet undetermined self-antigens. Therefore, the ability of HEL-specific CD4$^+$ CD25$^+$ T cells from 3A9 mice to suppress the pathogenicity of 3A9/G7mTg splenocytes indicates that Tregs and the cells that they controlled need not be directed to the same antigen. This is consistent with previous observations that Tregs can suppress T cells bearing other antigen specificities (16).

Discussion

To study tolerance induction of KRN T cells, we expressed its ligand, G7m, on APCs in the thymus and periphery. Through this Tg approach, APCs from G7mTg7 mice were 1,000-fold more potent in stimulating KRN T cells. Accordingly, we showed that such thymic overexpression resulted in T cell tolerance to GPI as demonstrated by deletion of >99% Vβ6$^+$ thymocytes, loss of GPI-specific T and B cell responses, and abrogation of arthritis. Unexpectedly, KRN/G7mTg7$^{k/g7}$ mice succumbed to an aggressive systemic autoimmune disease with multiorgan inflammation and autoantibody production. We showed further that the disease phenotype was not limited to the KRN mice but can also be elicited in 3A9 TCR Tg mice

bearing specificity for HEL. In both systems, systemic autoimmunity arose in the setting of massive thymic deletion with loss of transgene-encoded TCR specificity and diminution of $CD4^+$ $CD25^+$ Tregs. We propose that Tregs and autoreactive T cells can have differential susceptibility to tolerance induction, such that autoreactive T cells persist into the periphery. In the setting of lymphopenia, these cells undergo homeostatic proliferation to induce disease.

Thymic deletion is the major mechanism whereby autoreactive T cells are eliminated from the functional T cell repertoire. Incomplete thymic deletion allows autoreactive T cells to persist in the periphery where under certain conditions they are activated and cause disease. Mechanisms such as the induction of extrathymic deletion, anergy, and Tregs offer a buttress against the dangers of autoimmunity. In this study, we showed that the extremes of negative selection to a self-antigen can both result in autoimmunity and disease. In $KRN^{k/g7}$ mice, presentation of endogenous GPI was insufficient to effect complete deletion of KRN T cells resulting in their activation and arthritis through provision of T cell help to anti-GPI B cells. Overexpression of its TCR ligand G7m in the thymus deleted >99% of T cells with elimination of $CD4^+$ $CD25^+$ Tregs. Residual effector T cells bearing endogenously encoded TCRs with likely low affinity recognition for peripheral self-peptides escape thymic deletion and expand in the periphery through homeostatic proliferation and release from Treg inhibition to cause systemic disease.

KRN/G7mTg$^{k/g7}$ and 3A9/mHEL mice differed critically from the growing rank of systemic autoimmune disease models generated through targeted gene disruption, such as CTLA-$4^{-/-}$, TGFdnR, and IL-$10R^{-/-}$ mice (for review see reference 17) in that multiorgan systemic autoreactivity arose paradoxically in the setting of tolerance induction. Instead of the generalized lymphadenopathy and an expanded T cell compartment seen in the majority of these autoimmune models, KRN/G7mTg$^{k/g7}$ and 3A9/mHEL mice exhibited a paucity of T cells. The thymi and peripheral LNs were atrophic, an expected finding given the purposeful targeting of the antigen to sites mediating negative selection. As such, these mice more closely resembled autoreactivity associated with lymphopenia such as TCR $C\alpha^{-/-}$ and d3Ntx mice. Although KRN/G7mTg and 3A9/mHEL mice exhibited an ulcerative colitis-like disease as do the TCR $C\alpha^{-/-}$ mice (18), the disease in the KRN/G7mTg mice was more extensive affecting multiple organs and involving autoantibody production. The disease phenotype of KRN/G7mTg and 3A9/mHEL mice resembled the wasting disease described in neonatally thymectomized mice (19, 20). The mechanism of this autoimmunity has yet to be defined. In the more extensively studied d3NTx model of autoimmunity, autoimmune gastritis and oophoritis were mediated by T cells with specificity for peripherally expressed antigens: gastric parietal H^+/K^+ ATPase (21) and ovarian antigen (22), respectively. Autoimmunity to these peripheral antigens was attributed to the absence of thymically derived $CD4^+$ $CD25^+$ Tregs, whose restoration abrogated disease (14). Similarly, we showed here that depletion of $CD4^+$ $CD25^+$ Tregs conferred disease phenotype and the addition of $CD4^+$ $CD25^+$ Tregs prevented disease induction. In contrast to the surgical thymectomy models, we achieved such overwhelming thymocyte depletion via the thymic expression of a highly potent TCR ligand.

Numerous models of thymic tolerance had been described with diverse results. As allelic exclusion of transgene-encoded TCR was incomplete, coexpression of endogenously encoded TCRs allowed the generation of a repertoire of T cell specificities separate from those encoded by the transgenes. In some studies, coexpression of dual TCRs allowed autoreactive T cells to escape from negative selection and become activated upon recognition of their cognate antigen in the periphery to cause disease (23–26). In those cases, the autoreactivity was confined to that of the transgene-encoded TCR. Our system differed critically from these models in that the transgene TCR specificity was not required for disease as pathology can be elicited in recipient mice that do not express the cognate antigen. In other TCR systems, deletion in response to antigens such as superantigens resulted in no pathology. In accordance with previous observation, we found superantigen (Mls-1^a)-mediated deletion of KRN T cells to be delayed and less efficient. There was no ensuing disease (unpublished data). Yet other systems demonstrated the generation of Tregs through the recognition of self-peptide (27–30). Interestingly, it is weak recognition of self-peptide that gave rise to Tregs. As such, it is intriguing that $CD4^+$ $CD25^+$ Tregs are increased in $KRN^{k/g7}$ mice. One question that had been unanswered is why $KRN^{k/g7}$ mice were not subjected to systemic autoimmunity given the ubiquitous presentation of GPI. As we have shown, thymic presentation of GPI is insufficient to induce complete deletion of KRN T cells but does induce the development of GPI-specific $CD4^+$ $CD25^+$ Tregs, which may provide a mechanism whereby the autoreactivity is limited to humorally mediated joint-specific disease. Precedents of such modulation of autoaggression by Tregs had previously been demonstrated in the IDDM and experimental autoimmune encephalomyelitis models (31, 32). In the face of overwhelming antigen dose due to overexpression of a strong TCR agonist, Tregs may indeed be deleted. This is consistent with our observation that HEL-specific 3A9 TCR Tg mice also developed systemic autoreactivity when crossed to mHEL Tg mice. 3A9 T cells are exquisitely sensitive to HEL(46–61) and can be deleted by 10–100 HEL(46–61)–I-A^k complexes on APC surfaces (33). Thus, overly efficient deletion of 3A9 may eliminate Tregs from the repertoire. It is, therefore, the convergence of high ligand density and/or TCR binding affinity that results in T cell overstimulation and deletion. The requirement for these two factors to coexist may explain the lack of systemic autoreactivity seen in some but not all TCR systems (34–36). It is also possible that the TCR Tg mice were not followed for sufficient time for disease to manifest, as we had demonstrated with 3A9/JB5 mice.

What could account for the differential susceptibility of Tregs and pathologic effector T cells to deletion? Although

the mechanism of Tregs differentiation is yet unclear, selective loss of Tregs from the repertoire in B7.1/B7.2- (37) and Foxp3-deficient (10, 11) mice suggests that Tregs and effector T cells arise from different maturation programs. As Tregs required cognate interaction with their ligand for differentiation, they may exhibit higher affinity for self-peptide–MHC complex and thus be more susceptible to deletion compared with those expressing other autoimmune specificities to peripherally derived antigens. The preferential outgrowth of effector $CD4^+$ T cells using endogenously encoded Vβs provides support to this hypothesis. An alternative possibility is that Tregs and autoimmune T cells arise at a distinct time course in ontogeny as shown by d3Ntx models and represent different lineages. Therefore, they might be subjected to different selection pressures.

In addition to the loss of Tregs from the T cell repertoire, a critical component to the disease phenotype is the requirement for homeostatic proliferation as lymphopenia was a shared feature in both TCR/antigen models and d3NTx mice. However, the homeostatic proliferation is not indiscriminate as only $V\beta2^+$ T cells were selectively expanded in KRN/G7mTg7$^{k/g7}$ mice, suggesting that this expansion is antigen driven. Stimulation of $V\beta2^+$ T cells by BALB/cV virus in H-2^d and H-2^a had been previously reported correlating with deletion of $V\beta2^+$ T cells (38). No known endogenous Vβ2-specific superantigens had been found in B6 nor NOD mice, hence this expansion is unlikely to be superantigen related. Therefore, these cells represent endogenous autoreactive T cells that escape negative selection and in the setting of lymphopenia and absence of Tregs, cause systemic autoimmunity.

We thank Drs. K. Tung and M. LaRegina for histological review of the pathological samples, Drs. J.P. Atkinson, C. Pham, K. Tung, L. Norian, and E. Hailman for critical review of the manuscript, D. Kreamalmeyer, K. Matsui, R. DiPaolo, and J. Bui for technical assistance, and J. Smith for administrative assistance.

This work is supported by grants from the National Institutes of Health. F.F. Shih is supported by a grant from the Pediatric Scientist Development Program (National Institute of Child Health and Human Development).

Submitted: 10 July 2003
Accepted: 2 December 2003

References

1. Kouskoff, V., A.-S. Korganow, V. Duchatelle, C. Degott, C. Benoist, and D. Mathis. 1996. Organ-specific disease provoked by systemic autoimmunity. *Cell.* 87:811–822.
2. Basu, D., S. Horvath, I. Matsumoto, D.H. Fremont, and P.M. Allen. 2000. Molecular basis for recognition of an arthritic peptide and a foreign epitope on distinct MHC molecules by a single TCR. *J. Immunol.* 164:5788–5796.
3. Korganow, A.-S., H. Ji, S. Mangialaio, V. Duchatelle, R. Pelanda, T. Martin, C. Degott, H. Kikutani, K. Rajewsky, J.-L. Pasquali, et al. 1999. From systemic T cell self-reactivity to organ-specific autoimmune disease via immunoglobulins. *Immunity.* 10:451–461.
4. Wipke, B.T., and P.M. Allen. 2001. Essential role of neutrophils in the initiation and progression of a murine model of rheumatoid arthritis. *J. Immunol.* 167:1601–1608.
5. Ji, H., K. Ohmura, U. Mahmood, D.M. Lee, F.M.A. Hofhuis, S.A. Boackle, K. Takahashi, V.M. Holers, M.J. Walport, C. Gerard, et al. 2002. Arthritis critically dependent on innate immune system players. *Immunity.* 16:157–168.
6. Latek, R.R., A. Suri, S.J. Petzold, C.A. Nelson, O. Kanagawa, E.R. Unanue, and D.H. Fremont. 2000. Structural basis of peptide binding and presentation by the type I diabetes-associated MHC class II molecule of NOD mice. *Immunity.* 12:699–710.
7. Kouskoff, V., H.-J. Fehling, M. Lemeur, C. Benoist, and D. Mathis. 1993. A vector driving the expression of foreign cDNAs in the MHC class II-positive cells of transgenic mice. *J. Immunol. Methods.* 166:287–291.
8. Williams, C.B., K. Vidal, D.L. Donermeyer, D.A. Peterson, J.M. White, and P.M. Allen. 1998. In vivo expression of a T cell receptor antagonist: T cells escape central tolerance but are antagonized in the periphery. *J. Immunol.* 161:128–137.
9. Wipke, B.T., Z. Wang, J. Kim, T.J. McCarthy, and P.M. Allen. 2002. Dynamic visualization of a joint-specific autoimmune response through positron emmission tomography. *Nat. Immunol.* 3:366–372.
10. Khattri, R., T. Cox, S.-A. Yasayko, and F. Ramsdell. 2003. An essential role for Scurfin in $CD4^+CD25^+$ T regulatory cells. *Nat. Immunol.* 4:337–342.
11. Fontenot, J.D., M.A. Gavin, and A.Y. Rudensky. 2003. Foxp3 programs the development and function of $CD4^+$ $CD25^+$ regulatory T cells. *Nat. Immunol.* 4:330–336.
12. Smith, K.M., D.C. Olson, R. Hirose, and D. Hanahan. 1997. Pancreatic gene expression in rare cells of thymic medulla: evidence for functional contribution to T cell tolerance. *Int. Immunol.* 9:1355–1365.
13. Fritz, R.B., X. Wang, and M.-L. Zhao. 2000. Alterations in the spinal cord T cell repertoire during relapsing experimental autoimmune encephalomyelitis. *J. Immunol.* 164:6662–6668.
14. Sakaguchi, S., N. Sakaguchi, M. Asano, M. Itoh, and M. Toda. 1995. Immunologic self-tolerance maintained by activated T cells expressing IL-2 receptor α-chains (CD25). Breakdown of a single mechanism of self-tolerance causes various autoimmune diseases. *J. Immunol.* 155:1151–1164.
15. Asano, M., M. Toda, N. Sakaguchi, and S. Sakaguchi. 1996. Autoimmune disease as a consequence of developmental abnormality of a T cell subpopulation. *J. Exp. Med.* 184:387–396.
16. Thornton, A.M., and E.M. Shevach. 2000. Suppressor effector function of $CD4^+CD25^+$ immunoregulatory T cells is antigen nonspecific. *J. Immunol.* 164:183–190.
17. Marrack, P., J. Kappler, and B.L. Kotzin. 2001. Autoimmune disease: why and where it occurs. *Nat. Med.* 7:899–905.
18. Mombaerts, P., E. Mizoguchi, M.J. Grusby, L.H. Glimcher, A.K. Bhan, and S. Tonegawa. 1993. Spontaneous development of inflammatory bowel disease in T cell receptor mutant mice. *Cell.* 75:275–282.
19. Yunis, E.J., R. Hong, M.A. Grewe, C. Martinez, E. Cornelius, and R.A. Good. 1967. Postthymectomy wasting associated with autoimmune phenomena. I. Antiglobulin-positive anemia in A and C57BL-6 Ks mice. *J. Exp. Med.* 125:947–966.
20. Yunis, E.J., P.O. Teague, O. Stutman, and R.A. Good. 1969. Post-thymectomy autoimmune phenomena in mice. II. Morphologic observations. *Lab. Invest.* 20:46–61.
21. Suri-Payer, E., A.Z. Amar, R. McHugh, K. Natarajan, D.H. Margulies, and E.M. Shevach. 1999. Post-thymectomy autoimmune gastritis: fine specificity and pathogenicity of anti-

H/K ATPase-reactive T cells. *Eur. J. Immunol.* 29:669–677.
22. Alard, P., C. Thompson, S.S. Agersborg, J. Thatte, Y. Setiady, E. Samy, and K.S.K. Tung. 2001. Endogenous oocyte antigens are required for rapid induction and progression of autoimmune ovarian disease following day-3 thymectomy. *J. Immunol.* 166:4363–4369.
23. Zal, T., S. Weiss, A. Mellor, and B. Stockinger. 1996. Expression of a second receptor rescues self-specific T cells from thymic deletion and allows activation of autoreative effector function. *Proc. Natl. Acad. Sci. USA.* 93:9102–9107.
24. Riley, M.P., D.M. Cerasoli, M.S. Jordan, A.L. Petrone, F.F. Shih, and A.J. Caton. 2000. Graded deletion and virus-induced activation of autoreactive $CD4^+$ T cells. *J. Immunol.* 165:4870–4876.
25. He, X., C.A. Janeway, Jr., M. Levine, E. Robinson, P. Preston-Hurlburt, C. Viret, and K. Bottomly. 2002. Dual receptor T cells extend the immune repertoire for foreign antigens. *Nat. Immunol.* 3:127–134.
26. Sarukhan, A., C. Garcia, A. Lanoue, and H. von Boehmer. 1998. Allelic inclusion of T cell receptor α genes poses an autoimmune hazard due to low-level expression of autospecific receptors. *Immunity.* 8:563–570.
27. Jordan, M.S., A. Boesteanu, A.J. Reed, A.L. Petrone, A.E. Holenbeck, M.A. Lerman, A. Naji, and A.J. Caton. 2001. Thymic selection of $CD4^+CD25^+$ regulatory T cells induced by an agonist self-peptide. *Nat. Immunol.* 2:301–306.
28. Kawahata, K., Y. Misaki, M. Yamauchi, S. Tsunekawa, K. Setoguchi, J. Miyazaki, and K. Yamamoto. 2002. Generation of $CD4^+$ $CD25^+$ regulatory T cells from autoreactive T cells simultaneously with their negative selection in the thymus and from nonautoreactive T cells by endogenous TCR expression. *J. Immunol.* 168:4399–4405.
29. Tarbell, K.V., M. Lee, E. Ranheim, C.C. Chao, M. Sanna, S.-K. Kim, P. Dickie, L. Teyton, M. Davis, and H. McDevitt. 2002. $CD4^+$ T cells from glutamic acid decarboxylase (GAD)65-specific T cell receptor transgenic mice are not diabetogenic and can delay diabetes transfer. *J. Exp. Med.* 196: 481–492.
30. Apostolou, I., A. Sarukhan, L. Klein, and H. von Boehmer. 2002. Origin of regulatory T cells with known specificity for antigen. *Nat. Med.* 3:756–763.
31. Gonzalez, A., I. Andre-Schmutz, C. Carnaud, D. Mathis, and C. Benoist. 2001. Damage control, rather than unresponsiveness, effected by protective $DX5^+$ T cells in autoimmune diabetes. *Nat. Immunol.* 2:1117–1125.
32. Olivares-Villagómez, D., Y. Wang, and J.J. Lafaille. 1998. Regulatory $CD4^+$ T cells expressing endogenous T cell receptor chains protect myelin basic protein-specific transgenic mice from spontaneous autoimmune encephalomyelitis. *J. Exp. Med.* 188:1883–1894.
33. Peterson, D.A., R.J. DiPaolo, O. Kanagawa, and E.R. Unanue. 1999. Negative selection of immature thymocytes by a few peptide-MHC complexes: differential sensitivity of immature and mature T cells. *J. Immunol.* 162:3117–3120.
34. Kisielow, P., H. Blüthmann, U.D. Staerz, M. Steinmetz, and H. von Boehmer. 1988. Tolerance in T-cell-receptor transgenic mice involves deletion of nonmature $CD4^+8^+$ thymocytes. *Nature.* 333:742–746.
35. Oehen, S., L. Feng, Y. Xia, C.D. Surh, and S.M. Hedrick. 1996. Antigen compartmentation and T helper cell tolerance induction. *J. Exp. Med.* 183:2617–2626.
36. McGargill, M.A., D. Mayerova, H.E. Stefanski, B. Koehn, E.A. Parke, S.C. Jameson, A. Panoskaltsis-Mortari, and K.A. Hogquist. 2002. A spontaneous CD8 T cell-dependent autoimmune disease to an antigen expressed under the human keratin 14 promoter. *J. Immunol.* 169:2141–2147.
37. Salomon, B., D.J. Lenschow, L. Rhee, N. Ashourian, B. Singh, A. Sharpe, and J.A. Bluestone. 2000. B7/CD28 costimulation is essential for the homeostasis of the $CD4^+$ $CD25^+$ immunoregulatory T cells that control autoimmune diabetes. *Immunity.* 12:431–440.
38. Hodes, R.J., M.B. Novick, L.D. Palmer, and J.E. Knepper. 1993. Association of a V β2-specific superantigen with a tumorigenic milk-borne mouse mammary tumor virus. *J. Immunol.* 150:1422–1428.